Salt Effects on Hydrophobic Interaction and Charge Screening in the Folding of a Negatively Charged Peptide to a Coiled Coil (Leucine Zipper)†

Ilian Jelesarov,* Eberhard Dürr, Richard M. Thomas, and Hans Rudolf Bosshard*

Biochemisches Institut der Universität Zürich, Winterthurerstrasse 190, CH-8057 Zürich, Switzerland

Received December 3, 1997; Revised Manuscript Received March 20, 1998

ABSTRACT: The stability of a coiled coil or leucine zipper is controlled by hydrophobic interactions and electrostatic forces between the constituent helices. We have designed a 30-residue peptide with the repeating seven-residue pattern of a coiled coil, (**abcdefg**)$_n$, and with Glu in positions **e** and **g** of each heptad. The glutamate side chains prevented folding at pH values above 6 because of electrostatic repulsion across the helix dimer interface as well as within the individual helices. Protonation of the carboxylates changed the conformation from a random coil monomer to a coiled coil dimer. Folding at alkaline pH where the peptide had a net charge of $-7e$ was promoted by the addition of salts. The nature of the charge screening cation was less important than that of the anion. The high salt concentrations (>1 M) necessary to induce folding indicated that the salt-induced folding resulted from alterations in the protein−water interaction. Folding was promoted by the kosmotropic anions sulfate and fluoride and to a lesser extent by the weak kosmotrope formate, whereas chloride and the strong chaotrope perchlorate were ineffective. Kosmotropes are excluded from the protein surface, which is preferentially hydrated, and this promotes folding by strengthening hydrophobic interactions at the coiled coil interface. Although charge neutralization also contributed to folding, it was effective only when the screening cation was partnered by a good kosmotropic anion. Folding conformed to a two-state transition from random coil monomer to coiled coil dimer and was enthalpy driven and characterized by a change in the heat capacity of unfolding of 3.9 ± 1.2 kJ mol^{-1} K^{-1}. The rate of folding was analyzed by fluorescence stopped-flow measurements. Folding occurred in a biphasic reaction in which the rapid formation of an initial dimer ($k_f = 2 \times 10^7$ M^{-1} s^{-1}) was followed by an equally rapid concentration-independent rearrangement to the folded dimer ($k > 100$ s^{-1}).

The three-dimensional structure of a native protein results from a delicate balance between forces that either promote or oppose the compactly folded conformation. Major players in this thermodynamic interplay are hydrophobic, polar, and van der Waals interactions. In most cases, electrostatic attraction contributes only moderately to the folding free energy, while electrostatic repulsion strongly opposes folding. These effects involve not only charged groups within the protein but also interactions with charged cosolutes.[1] Indeed, such phenomena as salting-in and salting-out of proteins are the result of reciprocal interactions between solute, cosolute, and solvent water.

Simple and controllable model systems are helpful in resolving complex phenomena. The coiled coil motif possesses a well-defined three-dimensional structure, yet is small enough for controlled design (*1*). Coiled coils are found as structural motifs in proteins as diverse as tropomyosin, tRNA synthetase, influenza virus hemagglutinin, and transcriptional regulators (*2*). They consist of two or more peptides in an approximately α-helical conformation wound around each other. The structure is based on a recurring seven-residue motif, (**abcdefg**)$_n$, in which nonpolar aliphatic residues are frequent at **a** and **d** and charged residues at **e** and **g**. The main stabilizing forces originate from hydrophobic packing at the interface and from H-bonding. In addition, the stability is balanced by attractive and repulsive inter- and intrachain electrostatic forces. Crystal structures of leucine zippers, which are short coiled coils found in many transcription factors (*3*−*5*), indicate that a charged residue in position **g** of one strand can form a salt bridge with a residue of opposite charge in position **e′** [2] of the other strand (*6*, *7*). Salt bridges may or may not contribute to the stability of a coiled coil (*8*−*11*). Electrostatic repulsion between strands occurs when residues of like charge are juxtaposed across the coiled coil interface (*12*−*16*).

We have used model peptides to analyze the effect of electrostatics on the thermodynamics and kinetics of folding of coiled coils. In previous work we have studied the thermodynamics of folding of heterodimeric coiled coils composed of an acidic and a basic chain, either of which in isolation could not form a homodimeric coiled coil because of charge repulsion (*15*). When mixed together, the acidic and basic chains associated to a heterodimeric coiled coil in which the destabilizing repulsive charges were neutralized. The folding reaction could be described by an enthalpy-

† This work was supported in part by the Swiss National Science Foundation (Grant 3.45556.95).

* Authors to whom correspondence should be addressed.

[1] The nomenclature used is solvent = H_2O, protein = solute, salt = cosolute.

[2] The prime indicates a position in the opposite strand.

S0006-2960(97)02977-2 CCC: $15.00
Published on Web 05/02/1998

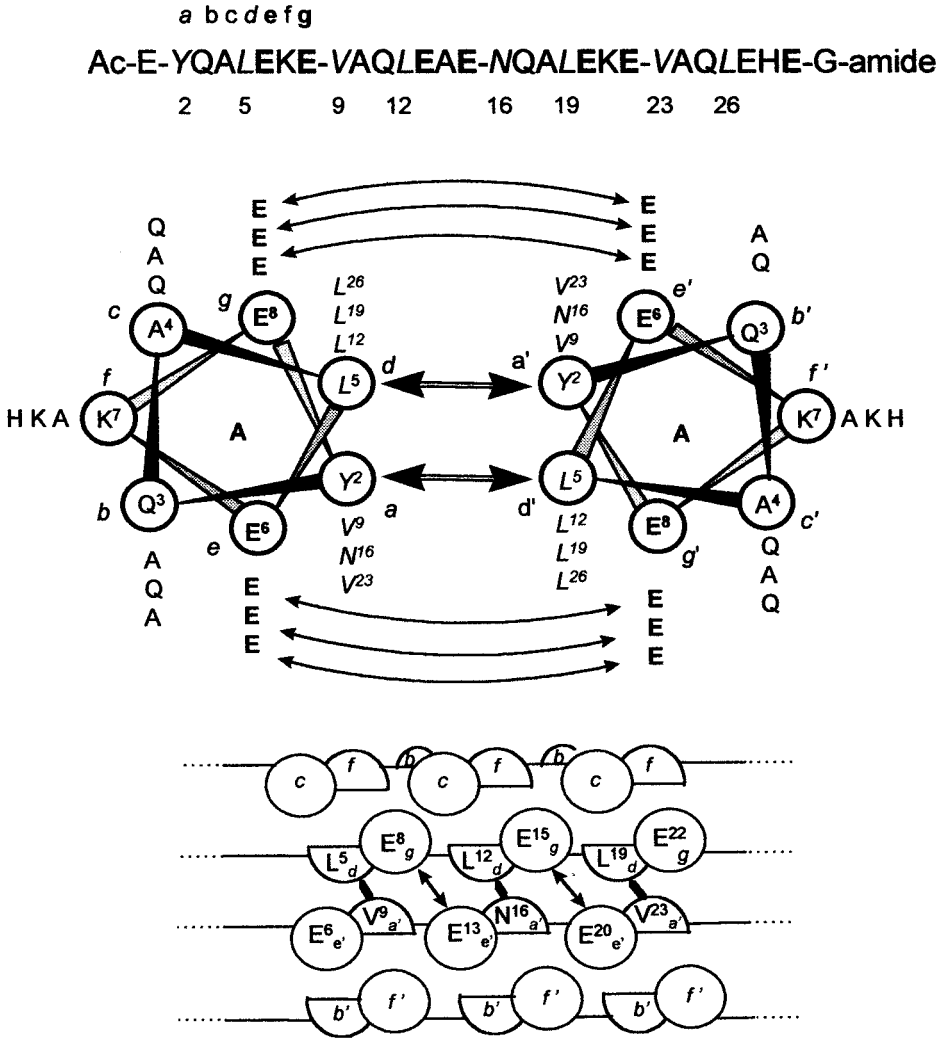

FIGURE 1: Sequence, helix wheel representation, and schematic structure of the parallel two-stranded coiled coil formed by peptide A. Sequence: Hydrophobic residues in heptad positions **a** and **d** are in italic, Glu's in positions **e** and **g** are in bold, heptads are separated by hyphens. Helix-wheel representation: Charge−charge repulsion between Glu's in the parallel dimeric coiled coil conformation are indicated by long, thin double-headed arrows, hydrophobic interactions at the interface of the two intertwined helices by short, thick double-headed arrows. Schematic 3D-structure: Each strand of the homodimeric, parallel coiled coil is drawn as a rod with the approximate position of the side chains indicated by spheres. Upper case letter indicates type of residue; lower case letter, position in heptad; number, sequence position; double-headed arrow, electrostatic repulsion; thick line, hydrophobic interaction. It is seen that residues in positions **b**, **c**, and **f** are facing the solvent-exposed outside of the coiled coil, whereas residues in positions **a**, **d**, **e**, and **g** contribute to the hydrophobic interface.

driven transition from a monomeric random coil structure to a dimeric coiled coil structure. The thermodynamic parameters of folding normalized per residue were of the same magnitude as for monomeric globular proteins, which indicated that the energetic balance of folding and association of a heterodimeric coiled coil was similar to that of the folding of a single polypeptide chain. Furthermore, folding was very rapid and ionic strength dependent (*16*).

Heterodimeric coiled coils are found in nature among the basic leucine zipper (bZIP) transcription factors. The variety of combinatorial interactions between different strands enables the control of function in these heterodimeric regulatory proteins (*5*, *17*−*19*). In view of the importance of homodimerization versus heterodimerization for the biological specificity of bZIP factors we ask the question: Can charge repulsion across the coiled coil interface be shielded? If so, is shielding caused by specific charge neutralization or by a general salt effect on the free energy of folding? Here we describe the cosolute-induced folding of the strongly acidic 30-residue peptide A (Figure 1). Small anions of high charge density, so-called kosmotropes,[3] induce the peptide to fold into a coiled coil by strengthening hydrophobic interactions. The nature of the charge-neutral-

[3] Kosmotropes are "water structure makers"; they are small ions of high charge density that bind water molecules tightly and increase the surface tension of aqueous solutions. Kosmotropes are preferentially excluded from the surface of the protein, which is preferentially hydrated. Typical kosmotropes are F^-, SO_4^{2-}, or Li^+. Kosmotropes stabilize proteins and decrease their solubility (salting-out). Chaotropes are large ions of low charge density that do not bind water but rather increase the mobility of nearby water molecules. Chaotropes destabilize proteins and increase their solubility (salting-in). Typical chaotropes are I^-, ClO_4^-, or Cs^+. Kosmotrope/chaotrope pairs are strongly dissociated and form highly soluble salts (e.g., KF). In general, chaotrope/chaotrope or kosmotrope/kosmotrope pairs are weakly dissociated and have low solubility (e.g., LiF, CsI), although the absolute free energies of hydration of ion pairs control their stability, and this can lead to selectivity series in which certain kosmotrope/chaotrope ion pairs are preferred to certain kosmotrope/kosmotrope or chaotrope/chaotrope ion pairs (*65*). For a detailed discussion, see refs *29*, *66*.

izing cation is less important. Folding is fast and can be described by a two-state transition from random coil to coiled coil at low peptide concentration.

EXPERIMENTAL PROCEDURES

Materials

Peptide Synthesis and Purification. Peptide A was synthesized on a 433A peptide synthesizer (Applied Biosystems), using the Rink amide MBHA resin (Novabiochem) and the 9-fluorenylmethyloxycarbonyl (N^{α}-Fmoc) protection strategy, as described before in detail (*16*, *20*). The peptide was released from the resin as the C-terminal amide. After desalting on a Sephadex-25 column in 1 M acetic acid, final purification was achieved by reversed phase high performance liquid chromatography on a semipreparative C8 column (Machery & Nagel) in binary gradients of acetonitrile/water containing 0.1 and 0.085% trifluoroacetic acid. Purity was controlled by amino acid analysis, and the calculated molecular mass was verified by ion spray mass spectrometry. 5-(and 6)-Carboxyfluorescein was attached to the free α-amino group of a variant of peptide A that had three additional N-terminal glycine residues. The fluorescein group was introduced before deprotection and cleavage of the peptide from the resin, by the reaction of the N-terminal α-amino group with 5-(and 6)-carboxyfluorescein-*N*-hydroxysuccinimidyl ester (Molecular Probes). Concentrations were determined from UV-absorption measurements in 6 M guanidinium hydrochloride, $\epsilon_{275.3\ nm} = 1450\ M^{-1}\ cm^{-1}$ (*21*). Concentrations are always expressed as total peptide concentration, e.g., 1 μM peptide corresponds to 0.5 μM dimeric coiled coil.

Methods

CD Spectroscopy. CD measurements were performed on a Jasco-715 spectropolarimeter equipped with a computer-controlled water bath, using a thermostated cuvette of 1 mm path length. Conformational changes induced by temperature, salt, or pH change were monitored by following the change in the α-helical band at 222 nm. Variation of pH in discrete steps was achieved by incubating 25 μM peptide in a buffer consisting of phosphoric acid, citric acid, and boric acid, 7.5 mM each, adjusted to the desired pH with NaOH or HCl and to a final total ionic strength of 0.1 M with KCl. Salt-induced folding was measured in 7.5 mM borate buffer adjusted to pH 9 after addition of the appropriate salt. Peptide concentration in these experiments was 20 μM and the samples were incubated for several hours before the CD measurements were made. The KF-induced transition was also followed by recording the CD spectrum between 240 and 185 nm at a scan rate of 1 nm min^{-1}. Temperature melting curves were measured for 5 different peptide concentrations from 2.5 to 90 μM, in 10 mM phosphate buffer, 3.7 M KF, pH ~ 9.4, at a heating rate of 1 °C min^{-1}. Reversibility was checked by reversed and repeated scans and was greater than 95%. Melting midpoints, T_m, were reproducible to within 1 K.

Kinetics of Coiled Coil Formation. Stopped-flow measurements were made on a SF-61 stopped-flow spectrofluorimeter (High Tech Scientific Ltd.) with a mixing dead time of 1−2 ms. Excitation was at 492 nm, and emission was measured above 530 nm (cutoff filter OG530). All experiments were performed at 25 °C in the 1:1 mixing mode to give the desired final peptide concentration (0.25−5 μM) in 10 mM phosphate, 4.4 M KF, pH ~ 9.5. Apparent rate constants were averaged from 10 to 12 individual kinetic traces, and each trace was the average of several syringe firings. In control experiments, no time-dependent change of the signal of the free fluorescein group was detected on transfer from buffer to KF solution.

Fluorescence Spectroscopy. Fluorescence measurements were performed on a Spex Fluorolog spectrofluorimeter at 20 °C. In one set of experiments the fluorescence of 20 μM peptide A in 10 mM phosphate buffer was measured in the absence and presence of 3.6 M KF. In another set of experiments 10 μM fluorescein-labeled peptide and 10 μM nonlabeled peptide were incubated in 3.6 M KF to allow strand exchange. The change in fluorescence emission was measured between 500 and 600 nm (excitation at 360 nm, 1 cm path length, 1 nm resolution, 2 s integration time).

Sedimentation Equilibrium. Conventional sedimentation equilibrium experiments were made with an XL-A analytical ultracentrifuge (Beckman, Palo Alto). Standard charcoal-filled Epon double sector centerpieces were used, and a sample volume of 120 μL was added to 30 μL of the fluorocarbon FC43 in the sample sector. Samples were exhaustively dialyzed against the relevant solvent before use. Experiments were conducted at between 35 000 and 45 000 rpm and at 20 °C. Data were acquired by averaging 20 radial scans at a spacing of 0.001 cm. Equilibration was confirmed by the superimposition of the concentration gradient measured after 24 and 48 h. A single species model was assumed and data were fit to the following equation:

$$c_r = c_0 \exp\{[M_{w,app}(1 - \bar{\nu}_2\rho)(r^2 - r_0^2)\omega^2]/2RT\} \qquad (1)$$

where $M_{w,app}$ is the apparent molecular mass, $\bar{\nu}_2$ is the partial specific volume, c is molal concentration, r is radial distance, and ρ is the solvent density. Density measurements were carried out with a DSA48 density and sound analyzer (Anton Paar, Graz, Austria) that was calibrated according to the manufacturer's instructions. All measurements were conducted at 20 °C and were made to a precision of $\pm 1 \times 10^{-4}$ g cm^{-3}. The partial specific volume ($\bar{\nu}_{20,c}$) of the peptide was calculated from the amino acid composition using published data (*22*) and an ad hoc computer program, and found to be 0.723 $cm^3\ g^{-1}$ at 20 °C. In the course of these investigations the dependence of the density of aqueous KF solutions ($\rho_{KF,20}$) as a function of salt concentration (X) at 20 °C was determined. The data could be best approximated by the following equation:

$$\rho_{KF,20} = A + BX + CX^2 \qquad (2)$$

where $A = 0.9987 \pm (4.7 \times 10^{-4})$, $B = 0.048 \pm (4.5 \times 10^{-4})$, and $C = -8.33 \times 10^{-4} \pm (9.1 \times 10^{-5})$, and where X is in moles $liter^{-1}$. This equation is valid from 0 to 4.5 M KF, and the maximum error was found to be 17.6×10^{-4} g cm^{-3}.

The isoionic point of peptide A is ~4.3, and it bears a net charge of $+3e$ at pH 2 and of $-7e$ at pH 8. The behavior of macroions sedimenting in a centrifugal field has been well

documented in the literature (*23*, *24*). From the results of this analysis it follows that

$$M_{\text{eff}} = M_2 - \frac{1}{2}ZM_3\frac{(1-\bar{\nu}_3\rho)}{(1-\bar{\nu}_2\rho)} \quad (3)$$

for an aqueous solution of a macroion PX_z in the presence of an electrolyte BX, where X is a small, univalent counterion. M_{eff} is the effective measured mass, M_2 is the true mass of the macroion, and M_3 is the mass of the cosolute. Following convention, subscripts 1, 2, and 3 refer to water, solute (macroion, i.e., coiled coil peptide), and cosolute (electrolyte), respectively. $\bar{\nu}_3$, the partial volume of the cosolute, at any concentration, c_3, can be estimated from a knowledge of the dependence of density on concentration for BX since (*22*, *25*)

$$\bar{\nu}_3 = \frac{1}{\rho_1}\left[1 - \left(\frac{\partial\rho_S}{\partial c_3}\right)\right] \quad (4)$$

where ρ_S is the solvent density. Equation 3 can then be simplified

$$M_{\text{w,app}} = M_2 - AZ \quad (5)$$

where $A = {}^1/_2M_3(1 - \bar{\nu}_3\rho)/(1 - \bar{\nu}_2\rho)$, which is constant for a given macroion at a fixed concentration of electrolyte. Full derivations of these equations are given in the literature (*23*, *24*).

RESULTS

Structure of Peptide A and Formation of a Coiled Coil at Low pH. The sequence of peptide A is shown in Figure 1. The pattern of hydrophobic residues in the heptad positions **a** and **d** was the same as in the natural leucine zipper domain of the yeast transcription factor GCN4, except for Tyr in the first **a**-position that served as a chromophore for the determination of peptide concentration. The pattern L^d V^a L^d N^a L^d V^a L^d (superscripts indicate positions in the heptad) with a central asparagine (N in position 16, Figure 1) stabilizes a parallel and in-register dimeric coiled coil (*19*, *26*−*28*). Helix-stabilizing residues were selected for the solvent-exposed positions **b**, **c**, and **f**.

Peptide A did not fold at neutral and alkaline pH values because of charge−charge repulsion between the glutamic acid residues in the **g** and **e** positions (Figures 1 and 2). In the coiled coil conformation, the side chain of the residue in the **g** position of one strand is close to the side chain of the residue in the **e′** position of the following heptad of the opposite strand, as indicated schematically in Figure 1. In the crystal of the GCN4 leucine zipper domain, pairs of Lys and Glu in positions (i, i'+5) are oriented in such a way that direct ionic bonds seem possible, although the ionic bonds may not actually exist in solution (*10*, *11*).

Protonation Induces Coiled Coil. To demonstrate that peptide A could adopt a helical structure when the negative charges were eliminated, the CD spectrum of peptide A was measured from pH 2 to 12. A plot of $[\theta]_{222}$ against pH showed a sharp transition with a midpoint at pH 5.2 (Figure 2). At neutral and alkaline pH, $[\theta]_{222}$ was near zero, as is typical of a random coil structure. $[\theta]_{222}$ dropped to −35 000 deg cm^2 dmol^{-1} in the acidic region, indicating that a fully helical conformation was adopted when the negative charges were eliminated. The value of $[\theta]_{222}$ at acidic pH was concentration dependent, as was to be expected in a noncovalently associating system (not shown).

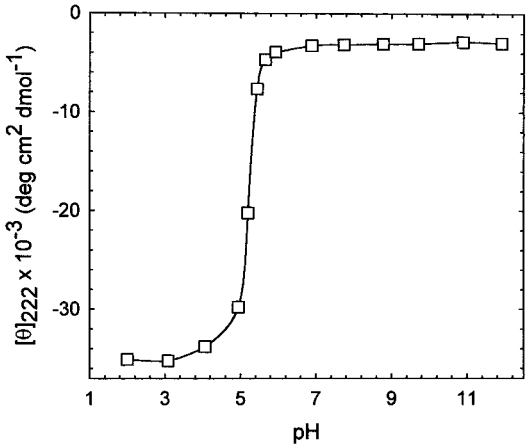

FIGURE 2: Change of the far-UV circular dichroism spectrum of peptide A with pH. The molar ellipticity per residue, $[\theta]_{222}$, is plotted against pH. Measurements were performed in 7.5 mM citrate-phosphate-borate buffer adjusted with HCl or KOH to the desired pH and with KCl to an ionic strength of 0.1 M. The total concentration of peptide was 25 μM and the temperature was 20 °C.

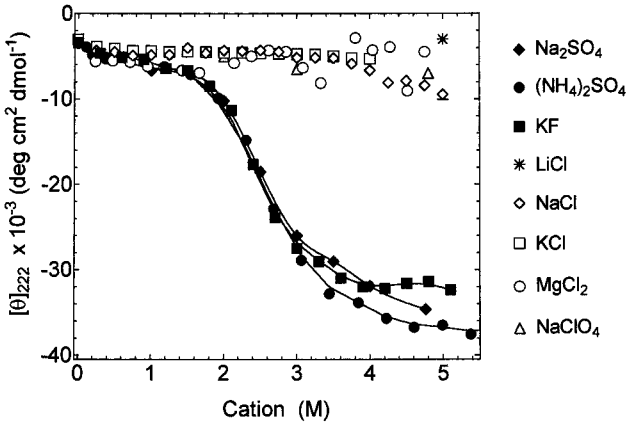

FIGURE 3: Titration of peptide A with different salts, as indicated. The molar ellipticity per residue, $[\theta]_{222}$, is plotted against the cation concentration. The total concentration of peptide was 20 μM in 7.5 mM borate buffer, pH 9, and 20 °C. Under these conditions, peptide A has a net charge of −8e.

Kosmotropic Salts Induce the Formation of a Coiled Coil. If protonation of the glutamate side chains induced a coiled coil, shielding of the negative charges by cations could have had the same effect. However, neither LiCl, NaCl, KCl, or $MgCl_2$ (Figure 3) nor RbCl or CsCl (not shown) promoted helix formation. In contrast, Na_2SO_4, $(NH_4)_2SO_4$, and KF (Figure 3) and also RbF and CsF (not shown) did induce a change in the CD spectrum corresponding to a random coil to helix transition.[4] Clearly, folding depended on the nature of the anion. Sulfate and fluoride, which promoted folding, are kosmotropic ions and are excluded from the protein

[4] Since HF is a weak acid, pK_a = 2.95 (*67*), concentrated fluoride salt solutions are basic. A 4 M KF solution has a pH of approximately 9.5. In our initial experiments, peptide A was dissolved in 10 mM potassium phosphate, pH 7.2, and the pH increased progressively when KF was added. In later experiments, peptide A was dissolved in 7.5 mM borate buffer, pH 9, to keep the pH between 9 and 9.5.

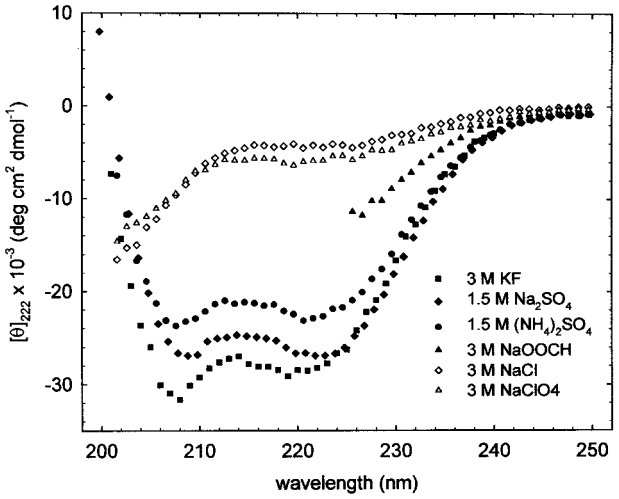

FIGURE 4: CD spectra of peptide A in the presence of different cations. The cation concentration was constant at 3 M. The total concentration of peptide A was 20 μM in 50 mM borate buffer of pH 9 and 20 °C. The spectrum in 3 M NaOOCH could be measured only down to 225 nm because of the very high optical absorption of formate below this wavelength.

surface. Proteins are preferentially hydrated in the presence of kosmotropes, which promote the burial of exposed hydrophobic groups and facilitate folding.[3] As a control we tested the weak kosmotropic anion formate and the strong chaotropic anion ClO_4^- (see ref *29* for the classification of kosmotropes and chaotropes). No folding was seen in 3 M $NaClO_4$, while 3 M sodium formate promoted only partial folding (Figure 4).

Chloride is neither a typical kosmotrope nor a chaotrope (*29*) but has been shown to partially inhibit α-helix formation in a neutral peptide (*30*). To test if the observed lack of folding in chloride was caused by this effect, the CD spectrum of peptide A in the presence and absence of 4 M NaCl was measured at pH 3 where peptide A is folded. NaCl had no effect on the helical CD spectrum of folded peptide A (not shown). We also checked the effect of 4 M NaCl on the helical CD spectrum of the neutral leucine zipper peptide GCN4p1 (*31*) and on the heterodimeric leucine zipper AB.[5] Again, 4 M NaCl did not induce a noticeable change of the CD spectrum (not shown). Hence, the inhibition of coiled coil formation by chloride per se can be ruled out.

Cation Effects. What effect had the nature of the cation? The carboxylates in peptide A have a high charge density (kosmotropic ions) and are best shielded by kosmotropic cations as kosmotrope/kosmotrope pairs are often strongly interacting.[3] Thus, one expects Li^+ or Mg^{2+} to be good shielding ions, but not NH_4^+, Rb^+, or Cs^+ (*29*). Unfortunately, it was not possible to test the entire series of fluoride salts because LiF and NaF are not sufficiently soluble to obtain concentrations higher than 1 M. However, the midpoint folding concentration of RbF and CsF was similar to that of KF (shown in Figure 3) and not higher, as would be the case if Rb^+ and Cs^+ were screening the negative charges less effectively. On the other hand, Na_2SO_4 was a somewhat stronger "folder" than $(NH_4)_2SO_4$, in agreement with weaker binding of the more chaotropic NH_4^+ to the carboxylate groups (Figure 4). However, the effect was small, and it was concluded that the nature of the neutralizing cation was of only minor importance for the folding behavior of peptide A.

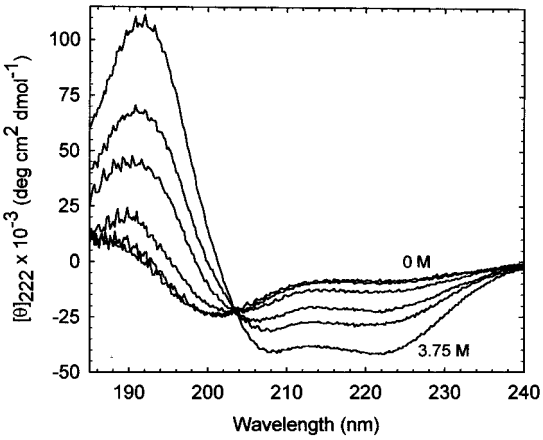

FIGURE 5: CD spectra of peptide A in the presence of increasing amounts of KF. The spectra shown are for 0, 0.5, 0.75, 1, 2, and 3.75 M KF. The total concentration of peptide A was 20 μM in 10 mM potassium phosphate, pH 7.2, and 20 °C. The pH increased on addition of KF and was approximately 9.4 at 3.75 M KF. The same spectral changes were measured when the pH was kept near 9 with borate buffer (not shown).

Salt-Induced Folding Followed a Two-State Transition from a Monomeric Random Coil to a Dimeric Coiled Coil. The change of the CD spectrum of peptide A measured at varying concentrations of KF exhibited an isodichroic point at 203 nm (Figure 5). The same isodichroic point was also seen in the thermal denaturation of the heterodimeric coiled coil AB[5] (*15*). An isodichroic point is taken as evidence for a transition between two conformational states in equilibrium with each other.

Equilibrium Sedimentation Analysis Indicates a Dimeric Coiled Coil. The residue pattern chosen for the **a** and **d** positions favors dimers (*19*, *26*−*28*). To confirm the stoichiometry, equilibrium sedimentation experiments were conducted at pH 2 where peptide A was protonated and in a coiled coil conformation, at pH 9 where it was a random coil, and in the presence of 3.5 M KF where it was a coiled coil. A difficulty encountered in the interpretation of the sedimentation equilibrium data was that the high net charge of the peptide and the presence of high concentrations of salt strongly affected the apparent molecular mass, $M_{w,app}$. Table 1 shows the $M_{w,app}$ of peptide A under a variety of solvent conditions as well as M_2, the mass corrected for charge and solute effects (see Methods). None of the $M_{w,app}$ in Table 1 are in agreement with the mass calculated from the amino acid composition (3468 Da) or multiples thereof. In solution at pH 8.0, $M_{w,app}$ is consistently lower than the compositional mass. At this pH the peptide is substantially deprotonated and bears a net charge of $-8e$. Ignoring the contribution of the buffering components, i.e., assuming that the peptide solution contains KF as the only cosolute, the parameter A (eq 5) can be calculated using the values of $\bar{\nu}_3$ computed from eq 4. The corrected mass M_2 has been estimated in this way, and the values are listed in Table 1. As can be seen, this treatment produces a result that is in good agreement with the calculated mass when the ionic strength is adjusted to 0.2−0.3 M. Conversely, assuming the compositional mass (3468 Da) of M_2 enables the

[5] The heterodimeric coiled coil AB is composed of peptide A (described in this paper) and peptide B that has the same sequence as peptide A, except that all **e** and **g** positions are occupied by Lys (*15*).

Table 1: The Apparent Molar Mass, $M_{w,app}$ of Peptide A in Different Solvent Conditions, and M_2, the Mass Corrected for Charge and Solute Effects (see the text for details)[a]

conditions	$M_{w,app}$	M_2
pH 8,[b] $I = 0.1$ M	2220 ± 30	2920
pH 8,[b] $I = 0.2$ M	2970 ± 30	3670
pH 8,[b] $I = 0.3$ M	2890 ± 30	3590
pH 2,[b] $I = 0.2$ M	6000 ± 60	6530
3.5 M KF (pH 9.5)	3900[c]	7050[d]

[a] The compositional molar mass of the monomeric peptide A is 3468 Da and that of the dimeric coiled coil is 6936 Da. [b] Phosphoric acid, citric acid, boric acid, 7.5 M each, pH adjusted with KOH or HCl, and ionic strength (I) with KCl. [c] $\phi'_2 = 0.723$ cm^3 g^{-1}. [d] $\phi'_2 = 0.790$ cm^3 g^{-1}.

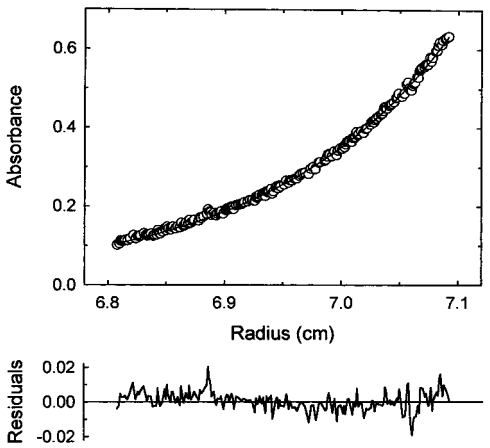

FIGURE 6: Representative sedimentation equilibrium profile. Peptide A (25 μM) in 7.5 mM citrate-phosphate-borate buffer, pH 2.0, and ionic strength 0.2 M, at equilibrium at 35 000 rpm and 20 °C. $M_{w,app}$ calculated from these data assuming the presence of a single ideal species (eq 1) is 6000 ± 60 Da, while the compositional molar mass of the dimer is 6936 Da. The residuals of the fit are indicative of a monomer−dimer equilibrium close to full association. Correction for charge effects yields $M_2 = 6530$ Da, indicating that protein A is indeed dimeric at pH 2 (see text for details).

computation of the absolute value of the effective charge, which was found to be $-5.5e$ to $-6.5e$ at ionic strength of 0.2−0.3 M. This seems a reasonable estimate, given that the formal net charge is $-8e$ under these conditions. The computed fit to the data measured at 0.1 M ionic strength was relatively poor, and the mass could not simply be corrected in the manner described. This suggests that under these conditions an insufficient concentration of electrolyte is present.

At pH 2.0, where all relevant side chains can be expected to be fully protonated, peptide A bears a net charge of $+3e$ and $M_{w,app}$ measured under these conditions is 6 kDa. The fit to the data (Figure 6) is reasonably good, although the form of the residual plot is reminiscent of that of a self-associating system close to full association. If the ionic strength is high enough, eq 3 can again be used to correct for the charge effect. The mass calculated in this way (6530 Da) is closer to that of a dimer (6936 Da). The CD data indicate that, at low pH, peptide A has an α-helical content of approx. 95%. If it is assumed that the fully associated form is 100% helical, the mass calculations confirm that the peptide is a dimer when fully associated.

The value of $M_{w,app}$ measured in 3.5 M KF reported in Table 1 was calculated using the compositional value of the partial specific volume (0.723 cm^3 g^{-1}). On first inspection it would seem that $M_{w,app}$ is close to that of the monomer. However, as was the case at pH 2, the residuals to the fit used to derive this quantity also appeared to indicate an incomplete association process. In a multicomponent system $\bar{\nu}_2$ is replaced by ϕ'_2, the isopotential apparent specific volume (*32*). This quantity can be determined by densimetric measurements on solutions at dialysis equilibrium under the relevant conditions. This measurement, which is notoriously difficult to perform accurately and requires high peptide or protein concentrations (*33*, *34*), has not been attempted for peptide A in 3.5 M KF. It has generally been found that ϕ'_2 increases with c_3 (*25*, *35*), and particularly marked effects of this kind have been found with proteins from halophilic bacteria at high (4−5 M) salt concentrations (*36*). Even for nonhalophilic proteins at moderate (1−2 M) salt concentrations, changes in the property ϕ'_2 of as high as ≈0.06 cm^3 g^{-1} have been reported (*25*, *33*). Adjusting ϕ'_2 for peptide A in 3.5 M KF by about this amount (i.e., setting $\phi'_2 = 0.79$ cm^3 g^{-1}) increases $M_{w,app}$ to 7050 Da, which is comparable to M_2 at pH 2.0 and suggests that peptide A also forms a dimer in concentrated KF solutions. While the assumptions made here are reasonable, it should be noted that results obtained from systems containing one electrolyte cannot necessarily be extended to others (*33*). Although peptide A has a high charge/mass ratio, changes in the partial volume due to electrostriction (*37*) have not been considered, as any effect is likely to be small in comparison with the features discussed above.

Parallel Orientation of Strands. The orientation of the two strands in the dimeric coiled coil was tested by fluorescence quenching experiments. N-terminal extension of a dimeric coiled coil by fluorescein-Gly-Gly-Gly produces a derivative whose fluorescence is quenched in the parallel, but not in the antiparallel orientation (*20*). Figure 7A shows that the fluorescence of peptide A with the fluorescein-Gly-Gly-Gly extension was quenched 3-fold and the emission maximum was shifted from 523 to 528 nm in the presence of 3.6 M KF, supporting a parallel orientation of strands. When solutions of fluorescein-labeled and nonlabeled parallel coiled coils are mixed, the fluorescence increases because of the exchange of fluorescent and nonfluorescent strands (*20*).[6] Labeled and nonlabeled coiled coils of the same concentration were mixed at a volume ratio of 1:1 so that the monomer/dimer equilibrium was not shifted. As a result, the fluorescence increased, again supporting the parallel arrangement of strands (Figure 7B).

The thermodynamics and kinetics of folding of the KF-induced coiled coil were then analyzed in more detail.

Analysis of the Fluoride-Induced Transition by the Linear Extrapolation Method. Folding/unfolding of proteins by denaturants can be analyzed by assuming a linear relationship between the free energy of unfolding and the concentration of denaturant according to $\Delta G_U = \Delta G_U{}^W - m$[denaturant] (*38*). ΔG_U is the free energy of unfolding in denaturant, and $\Delta G_U{}^W$ is the corresponding value obtained by extrapolation to zero denaturant concentration. The slope m has a

[6] No fluorescence increase is seen after the exchange of anti-parallel strands because the microenvironment of the unpaired N-terminal fluorescein group in an anti-parallel coiled coil does not alter during strand exchange.

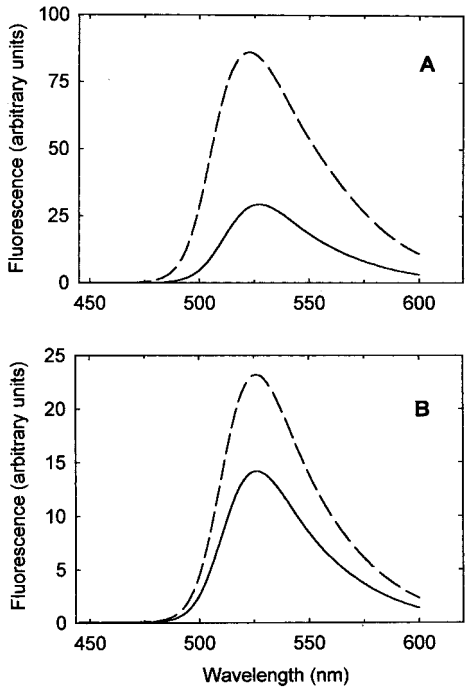

FIGURE 7: Parallel orientation of strands in the dimeric coiled coil is demonstrated by fluorescence quenching in peptide A with the N-terminal extension fluorescein-Gly-Gly-Gly. (A) Fluorescence spectra of 20 μM peptide A in the absence (dashed line) and in the presence (solid line) of 3.6 M KF. The quenching of the fluorescence and the shift of the emission maximum are caused by self-quenching between neighboring chromophores in the parallel orientation. (B) Strand exchange between peptide A and fluorescein-labeled peptide A confirms the parallel orientation of strands. The fluorescence emission of 10 μM fluorescein-labeled peptide A alone (solid line) is lower than the emission of a mixture of 10 μM each of the fluorescent and nonfluorescent peptides (dashed line). The fluorescence increase is caused by strand exchange between the fluorescent and nonfluorescent dimers to produce a heterodimer with only one strand containing an unpaired fluorescein group, which emits more strongly compared to the paired fluorescein groups in the homodimer.

negative value since ΔG_U decreases with increasing denaturant concentration. Applying this analysis to the salt-dependent folding/unfolding of peptide A, we write

$$\Delta G_U = \Delta G_U{}^W + m[\text{salt}] \quad (6)$$

In eq 6, $\Delta G_U W$ is the free energy of unfolding extrapolated to [salt] = 0. The slope m will have a positive value because salt stabilizes the folded conformation and, therefore, ΔG_U increases with increasing [salt]. The unfolding equilibrium constant is defined as $K_U = [M]^2/[D]$, where [M] is the concentration of the random coil monomer and [D] that of the coiled coil dimer. K_U was calculated from the change in the mean residue ellipticity at different salt concentrations using the relationship (*39*)

$$K_U = \frac{2[\text{peptide}]_{tot} f_U{}^2}{1 - f_U} \quad (7)$$

where $[\text{peptide}]_{tot}$ is the total peptide concentration, and f_U is the fraction of random coil monomer obtained from

$$f_U = \frac{\Delta[\theta]}{\Delta[\theta]_{max}} \quad (8)$$

$\Delta[\theta] = [\theta] - [\theta]_D$, where $[\theta]$ is the measured mean residue ellipticity and $[\theta]_D$ is the mean residue ellipticity of the coiled coil dimer. $\Delta[\theta]_{max} = [\theta]_M - [\theta]_D$, where $[\theta]_M$ is the mean residue ellipticity of the random coil monomer. Typical CD data used to calculate f_U are shown in Figure 8A. A correction was made for the linear dependence of $[\theta]_D$ and $[\theta]_M$ on the salt concentration (*15*, *38*) (dotted lines in Figure 8A). Figure 8B shows a plot according to eq 6 for values in the range $0.1 < f_U < 0.9$. The data extrapolate to $\Delta G_U{}^W = -2.6 \pm 0.15$ kJ/mol, in agreement with the observation that the equilibrium favored the random coil monomer in the absence of salt. Extrapolation to 3.7 M KF, the salt concentration at which peptide A is ≈100% folded (Figure 8A), gives $\Delta G_U = 38.5$ kJ/mol. The validity of this value was tested by thermal denaturation experiments.

Thermal Denaturation of the Fluoride-Induced Coiled Coil. Thermal denaturation of the coiled coil was concentration dependent. Thermal unfolding curves in 3.7 M KF for five different concentrations are shown in Figure 9. The fraction f_U was calculated from the temperature dependence of $[\theta]_{222}$ as described above for the salt dependence of $[\theta]_{222}$. ΔH_m, the enthalpy of unfolding at the midpoint temperature T_m of the unfolding curve, was obtained from a van't Hoff plot over the range $T_m \pm 2.5$ °C. The relationship between ΔH_m and T_m is shown in the inset of Figure 9. The plot is linear within the limit of error. The slope corresponds to the heat capacity change of unfolding and has a value of $\Delta C_p{}^{unf} = 3.9 \pm 1.2$ kJ mol^{-1} K^{-1}. As a further test of the validity of the two-state transition described by eq 7, $\ln[\text{peptide}]_{tot}$ was plotted against T_m. In agreement with a two-state transition (*15*, *39*) this plot was also linear (not shown).

The temperature stability curve of the coiled coil induced by 3.7 M KF is shown in Figure 10. The curve was calculated from

$$\Delta G_U = \Delta H_m\left(1 - \frac{T}{T_m}\right) + \Delta C_p{}^{unf}\left[T - T_m - T\ln\left(\frac{T}{T_m}\right)\right] - RT\ln[\text{peptide}]_{tot} \quad (9)$$

with $\Delta H_m = 188$ kJ/mol at $T_m = 316.6$ K (data for 50 μM peptide in Figure 9) and $\Delta C_p{}^{unf} = 3.9$ kJ mol^{-1} K^{-1} (inset of Figure 9). The last term in eq 9 corrects for the concentration dependence of ΔG_U (*15*, *39*). From the calculated stability curve one obtains $\Delta G_U = 37.7$ kJ/mol at 20 °C. This value is in excellent agreement with $\Delta G_U = 38.5$ kJ/mol predicted by the linear dependence of ΔG_U on KF concentration measured at 20 °C (Figure 8B).

Kinetics of Salt-Induced Folding. Peptide A with a N-terminal fluorescein group was used to measure the folding kinetics after the peptide was rapidly diluted into 4.4 M KF. Under these high salt conditions, folding was very rapid and the back reaction (dissociation into monomers) could be neglected. In the simplest case, the formation of the coiled coil is described by

$$2M \xrightarrow{k_f} D \qquad -\frac{d[M]}{dt} = k_f[M]^2 \quad (10)$$

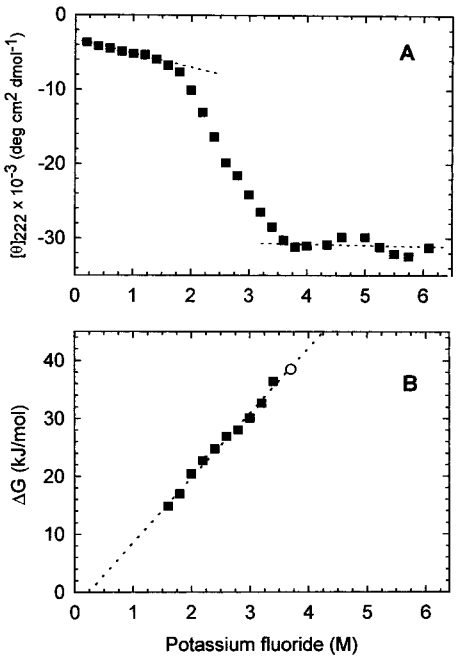

FIGURE 8: Change of the mean residue ellipticity at 222 nm as a function of KF concentration (A) and linear relationship between ΔG_U and the concentration of KF (B). ΔG_U was calculated from the data in panel A as described in the text and was plotted according to eq 6. The plot in panel B extrapolates to $\Delta G_U{}^W = -2.6 \pm 2$ kJ/mol and has a slope of $m = 11.2 \pm 1.5$ kJ mol^{-1} M^{-1} per residue. Experiments were performed at 20 °C with 20 μM peptide A. The open circle in panel B shows $\Delta G_U = 38.5$ kJ/mol at 20 °C and 3.7 M KF, the salt concentration at which folding was complete.

where k_f is a bimolecular rate constant. The fluorescence decreased when the monomers associated to the dimer because the fluorescence was quenched in the parallel coiled coil (Figure 7). The time-dependent decrease of fluorescence is

$$F(t) = \Delta F_{max}\left(\frac{[M]}{[M]_0}\right) + F_\infty \qquad (11)$$

$[M]_0$ is the concentration of the monomer at time zero and is equivalent to the total peptide concentration if the initial concentration of salt is zero ($[M] = [M]_0$). ΔF_{max} is the maximum change of fluorescence (equivalent to the fluorescence change from monomer to dimer) and F_∞ is the fluorescence at infinite time (after complete folding). Integration of eq 10 and combination with eq 11 gives

$$F(t) = \Delta F_{max}\left(\frac{1}{1 + k_{obs}t}\right) + F_\infty \qquad (12)$$

with

$$k_{obs} = k_f[M]_0 \qquad (12a)$$

Peptide A in 10 mM phosphate was mixed with concentrated KF (final concentration 4.4 M) in the stopped-flow instrument. The time course of the fluorescence decrease was well-fitted by eq 12 (Figure 11A). Hence, under the chosen conditions the coupled association and folding of two random coil peptide chains to a folded coiled coil dimer was described adequately by a single reaction phase. Equation 12a predicts that the observed rate constant should depend linearly on the total peptide concentration. As a test, the folding was measured using peptide concentrations from 0.25 to 5 μM. Figure 11B shows that the increase of k_{obs} with the peptide concentration was not linear over the entire concentration range. However, at the highest concentration (5 μM) the reaction was very fast and the value of k_{obs} could have been in error because the dead time of mixing was significant compared to the duration of the entire reaction. Therefore, the data were refitted omitting the initial 10 ms of the reaction. This did not increase k_{obs} and, hence, the deviation from linearity seen in Figure 11B was real. One possibility was that, as the bimolecular association became faster, a unimolecular reaction began to contribute to the observed rate. In principle, a co-rate limiting unimolecular reaction may either precede or follow the bimolecular reaction. But since the fluorescence decrease was caused by the juxtaposition of the N-terminal fluorescein groups in the coiled coil dimer, it seemed very unlikely that the unimolecular reaction preceded the association reaction. Therefore, one may explain the nonlinear plot of Figure 11B by a two-step reaction in which the first step corresponds to the association of two monomers to a partly folded dimer (encounter complex) and the second step to a rearrangement of the encounter complex to the stable coiled coil. The initial slope in Figure 11B yields a bimolecular rate constant of approximately 2×10^7 M^{-1} s^{-1}. This is only 1 to 2 orders of magnitude slower than the diffusion limit (*16*). The subsequent unimolecular rearrangement is also fast and only becomes rate-limiting at peptide concentrations above 5 μM, the highest concentration tested. Hence, the rate constant of the unimolecular reaction is probably much higher than 100 s^{-1}.

DISCUSSION

Electrostatic Effects and Coiled Coil Stability. A large body of work on natural and artificial coiled coils indicates that attractive and repulsive electrostatic forces across the dimer interface are delicately balanced. As an example, the *Fos* protein does not dimerize well because of intermolecular electrostatic repulsions, but it forms a stable heterodimer with the *Jun* protein (*40*). The energetic contribution of ionic bonds seems to be small because the gain in electrostatic energy is partly compensated by a loss in the hydration energy of the charged amino acid side chains (*8*, *10*). Model studies have shown that electrostatic attraction is not always necessary for the formation of a coiled coil (*9*, *14*, *41*, *42*). On the other hand, the formation of a coiled coil by protonated peptide A confirms previous studies by others. For example, a disulfide-linked coiled coil with several Glu's in positions **e** and **g** (*43*) was stabilized by protonation, which not only removed the repulsive charges but also increased the hydrophobicity of the side chains, thereby decreasing the energetic penalty of dehydration of the side chains (*9*, *14*, *42*). Stabilization through protonation of carboxylate groups has also been observed for the globular protein β-lactoglobulin (*44*).

The high glutamic acid content of peptide A gives it some resemblance to halophilic proteins (*37*), which is mirrored in its behavior at high salt concentration and suggests that it might be of use as a simple model of such proteins. The mechanism of the stabilization of halophilic proteins by salt

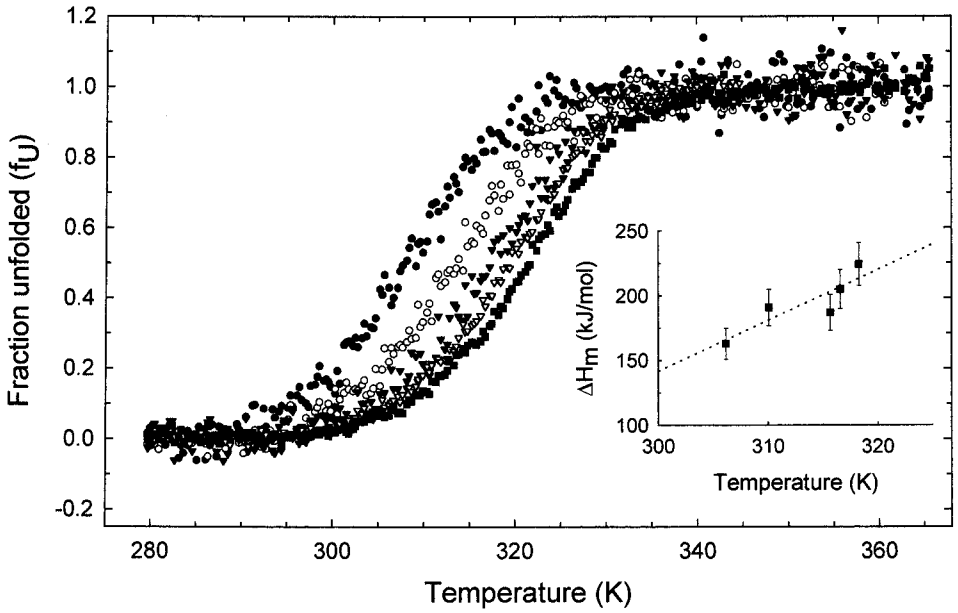

FIGURE 9: Thermal unfolding of the coiled coil induced by 3.7 M KF. Experiments were performed with (from left to right) 2.5, 10, 22, 50, and 90 μM peptide in the presence of 3.7 M KF. Inset: Plot of the enthalpy change at the midpoint temperature of unfolding against T_m. The dotted line is a best fit with slope $\Delta C_P^{unf} = 3.9 \pm 1.2$ kJ mol^{-1} K^{-1}.

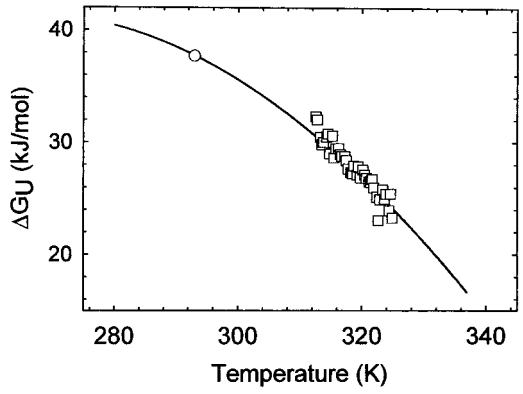

FIGURE 10: Temperature stability curve for the dimeric coiled coil conformation of peptide A in 3.7 M KF. The solid line was calculated according to eq 9 using the data for 50 μM peptide in Figure 9 and $\Delta C_P^{unf} = 3.9$ kJ mol^{-1} K^{-1}. Experimental data from Figure 9 are shown for temperatures in the range $T_m \pm 2.5$ °C. The open circle shows $\Delta G_U = 37.7$ kJ/mol at 20 °C, in excellent agreement with $\Delta G_U = 38.5$ kJ/mol predicted from the linear change of ΔG_U with KF (Figure 8B).

have been reviewed recently (*45*) as have general aspects of the interaction of proteins with solvent components (*46*).

Salt Effects on Protein Stability. The effect of salt on stability is complex. Salt may directly bind to various functional groups, or it may act indirectly by interacting with the solvent water. In a seminal paper von Hippel and Wong (*47*) proposed more than 30 years ago that the stabilizing and destabilizing effect of neutral salts is connected with interaction of salt and solvent molecules and can be understood in the framework of the Kauzmann−Némethy−Scheraga−Tanford view of hydrophobic bonding (*48*−*50*). In this view, the folded form of the protein is stabilized with respect to the unfolded form largely by the unfavorable free energy of transfer of the nonpolar side chains from the interior of the folded protein to the surrounding water. The main contribution to the positive ΔG of unfolding is the large negative entropy of apolar hydration. It more than compensates for the increase of conformational entropy on unfolding and, in general, dominates all other entropic effects involved in protein unfolding. As a consequence, the total entropy of the system decreases when the protein unfolds.

In a similar vein and at about the same time the cavity theory was formulated to explain the enhanced stability of the DNA double helix and of proteins in aqueous salt solutions as compared to organic solvents (*51*, *52*). According to the cavity theory, a major factor in stabilizing the folded form of a protein is the free energy required to form a cavity in the solvent to accommodate the protein (or DNA) molecule. This energy (ΔG_{cav}) is larger for the unfolded protein in which a larger fraction of nonpolar residues are exposed to water, than for the folded protein in which the nonpolar residues are buried in the interior. In the presence of kosmotropic ions,[3] the free energy is even more unfavorable for a hydrophobic group to stay exposed to the salt solution because the protein is preferentially hydrated. In this way, the protein-stabilizing kosmotropic ions act as an important driving force for the burial of hydrophobic groups.

With these general considerations in mind we partition ΔG_U, the free energy of unfolding of the coiled coil, as follows:

$$\Delta G_U = \Delta G_{hy} + \Delta G_{el} + \Delta G_{other} \qquad (13)$$

ΔG_{hy} is the hydrophobic and ΔG_{el} the electrostatic contribution to the unfolding free energy. ΔG_{other} lumps together all other contributions such as the free energy changes caused by H-bonds, van der Waals interactions, conformational changes, and statistical effects (e.g., cratic entropy, owing to the monomer/dimer transition). In the absence of salt and at pH > 6, ΔG_U was negative (equilibrium favors unfolded monomer). Since ΔG_{hy} was positive at moderate temperature (exposure of hydrophobic groups was disfavored), the major favorable contribution to ΔG_U came from a strongly negative ΔG_{el}, that is, from the sequestering of the negative charges

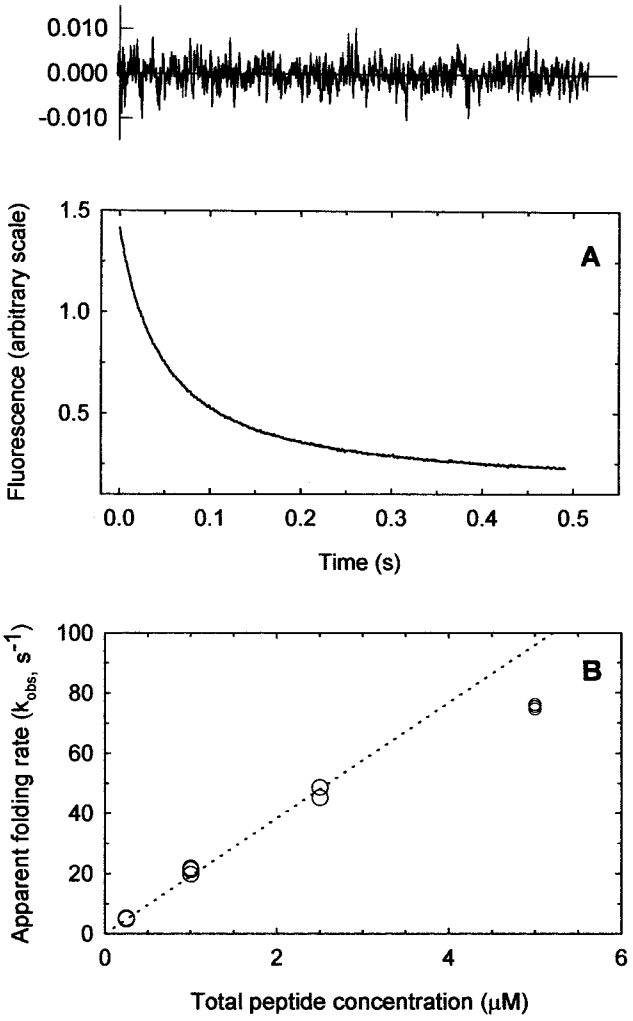

FIGURE 11: Folding reaction observed by fluorescence stopped-flow experiment (A) and dependence of observed rate of folding (k_{obs}) on the total peptide concentration (B). (A) Folding was achieved by a stopped-flow mixing from 0 to 4.4 M KF. The final protein concentration was 1 μM. The solid line is a best fit according to eq 12 with $k_{obs} = 21.3\ s^{-1}$, $\Delta F_{max} = 1.48$ and $F_\infty = 0.12$. The residuals of the fit shown at the top are very small and show no systematic trend, indicating that the association reaction is described adequately by a single phase transition. (B). Plot of the observed rate constant against the total peptide concentration during folding. The dotted line is a best fit to eq 12a for eight experiments in the range 0.25 to 2.5 μM peptide. The slope of the line is $k_f = 1.9 \times 10^7\ M^{-1}\ s^{-1}$.

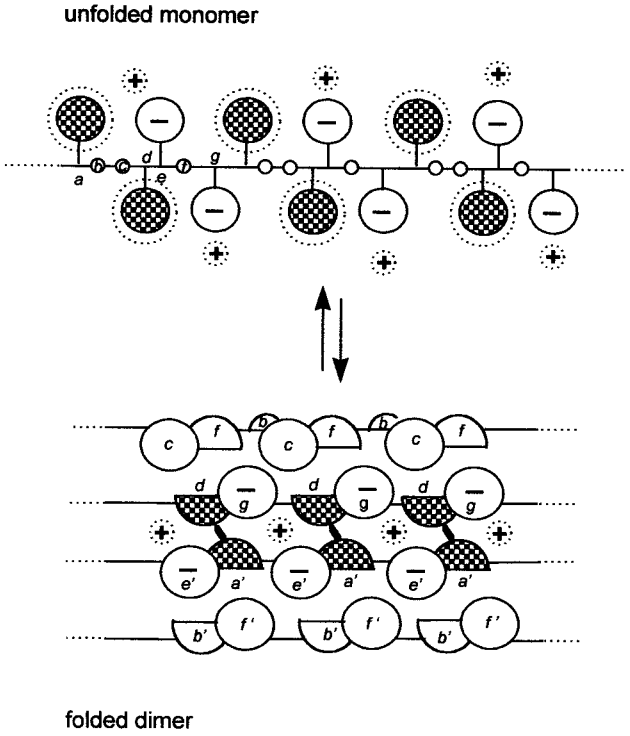

FIGURE 12: Schematic diagram of the transition from a random coil monomer to a coiled coil dimer. Crosshatched balls indicate hydrophobic residues in positions **a** and **d**; dotted circles, layers of ordered water molecules around solvent-exposed hydrophobic residues in the unfolded peptide; circles with minus sign, Glu in positions **e** and **g**; small dotted circles with plus sign, cations. See text for further explanation.

in the unfolded monomer (Figure 12). ΔG_{other} can be neglected because the different contributions to ΔG_{other} tend to cancel, and ΔG_{other} is small in comparison to ΔG_{hy} and ΔG_{el} (*53*, *54*).

On addition of fluoride or sulfate, ΔG_U increased and eventually became positive, shifting the equilibrium to the coiled coil. This can be explained, according to the cavity theory, by an increase in ΔG_{hy} because cavity formation around the exposed hydrophobic side chains was even more disfavored in the presence of salt than in pure water. We may write

$$\Delta G_U = -\Delta G_{cav} + \Delta G_{el} + \Delta G_{other} \qquad (13a)$$

where $-\Delta G_{cav} = \Delta G_{hy}$. That is to say, the increase of ΔG_{hy} is regarded to be a consequence of the decrease of ΔG_{cav}. In addition, an increase in ΔG_{el} through charge screening in the coiled coil will have further contributed to a positive value of ΔG_U.

Stabilization by Charge Screening. Why was folding not induced by charge screening with Na^+, K^+, or Mg^{2+} without a strongly kosmotropic counterion? A likely explanation is the high negative charge of peptide A above pH 6 which would lead to eight repulsive ion pairs in a noncovalently stabilized coiled coil. Neutralization of repulsive charges by KCl was found to induce folding of an acidic coiled coil peptide that was disulfide-linked (*13*, *43*). However, in this case, the formation of the coiled coil was not a concentration-dependent association of two unfolded monomeric peptide chains present at micromolar concentrations but was akin to the folding of a single polypeptide chain. The effective concentration of the associating disulfide-linked chains was several orders of magnitude higher, probably in the millimolar range (*55*). This could explain the induction of folding by charge screening observed with the disulfide-linked acidic model leucine zippers (*13*). In another recent study, a strongly basic peptide with the heptad pattern $(VKKLAKA)_n$ was induced to form a coiled coil by less than 0.5 M $NaClO_4$ (*56*). The positively charged lysine side chains in $(VKKLAKA)_n$ face the outside of the coiled coil and are less conformationally restricted than the Glu's in peptide A. Moreover, screening of the ammonium group of the lysine side chain by ClO_4^- yields a stable chaotrope/chaotrope pair.

We know of only one other study reporting on the effect of different halides on the folding of a coiled coil: folding of the leucine zipper domain of GCN4 was found to depend

on the nature of the anion in the order $F^- > Cl^- > Br^-$ (*57*). The stabilizing fluoride effect was ascribed to specific anion binding. Although this may have assisted folding of the neutral GCN4 leucine zipper peptide, which has acidic and basic residues in the **e** and **g** positions, an enhanced hydrophobic effect in the presence of fluoride may have been the main contributor to the folding of GCN4, the more so as the above order of anions matches the order of decreasing kosmotropic character (*29*).

Heat Capacity Change. Large positive heat capacity changes are typical of transitions from folded to unfolded proteins (*58*−*60*). ΔC_P^{unf} empirically correlates with an increase in the solvent-accessible apolar and polar surface on going from the native compact state to the denatured state (*53*). ΔC_P^{unf} for the KF-induced coiled coil was 3.9 ± 1.2 kJ mol^{-1} K^{-1}, corresponding to 65 J K^{-1} $(mol\ residue)^{-1}$. This value is quite large, yet lies in the range of values measured for the unfolding of much larger monomeric proteins (*60*). In previous work we have estimated $\Delta C_P^{unf} = 3-4$ kJ K^{-1} mol^{-1} for a closely related heterodimeric coiled coil (*15*). This result, together with ΔC_P^{unf} obtained here, demonstrates that the tightly packed hydrophobic core in the small rod-shaped coiled coil matches the thermodynamic stability typical of larger globular proteins.

Folding Kinetics Induced by Salt. Folding induced by KF was very rapid. The second-order rate constant of 2×10^7 M^{-1} s^{-1} was about 100 times higher than that reported for the folding of the leucine zipper domain of the transcription factor GCN4 (*61*) and for synthetic model coiled coils (*20*). Equally rapid folding was seen only with a heterodimeric coiled coil composed of an acidic and a basic peptide chain (*16*). In this case, the rapid folding rate was ascribed to electrostatic attraction between the two peptides, which, however, cannot explain rapid folding of peptide A in KF. The high folding rate may be caused by a very rapid hydrophobic collapse in KF solution (*62*, *63*).

The helices are only stable when folded in the coiled coil conformation and not as individual monomeric peptides. Therefore it is to be expected that two unfolded monomers cannot associate to the folded dimer in a single step and, hence, the minimal two-step mechanism deduced from the concentration dependence of the observed rate constants is reasonable. We have observed two-step folding for the GCN4 leucine zipper (*31*) and for synthetic model coiled coils (*20*). Two-step folding was reported for the very long coiled coil of tropomyosin (*64*). However, folding may appear monophasic if a kinetic intermediate is very short-lived or if its concentration is very low (*16*, *61*). Folding of peptide A was apparently monophasic at low peptide concentrations where the rearrangement step was not yet co-rate limiting.

In conclusion, the present work illustrates how salt can override electrostatic repulsion in a coiled coil. An important finding is that the neutralization of repulsive charges alone may not always suffice to induce folding. In the case of the very acidic peptide A, folding was accomplished only when the charge-shielding cations were added together with a protein-stabilizing kosmotropic anion. The results emphasize the delicate interplay between electrostatic and hydrophobic effects in protein folding and how they are influenced by interactions between protein, low-molecular-weight solute, and solvent.

ACKNOWLEDGMENT

We thank Antonio Baici for help with the stopped-flow experiments.

REFERENCES

1. Hodges, R. S., Semchuk, P. D., Taneja, A. K., Kay, C. M., Parker, J. M. R., and Mant, C. T. (1988) *Pept. Res. 1*, 19−30.
2. Lupas, A. (1996) *Trends Biochem. Sci. 21*, 375−382.
3. Hope, I. A., and Struhl, K. (1987) *EMBO J. 6*, 2781−2784.
4. Landschulz, W. H., Johnson, P. F., and McKnight, S. L. (1988) *Science 240*, 1759−1764.
5. Hurst, H. C. (1996) *Leucine Zippers: Transcription factors*, Academic Press, London.
6. Alber, T. (1992) *Curr. Opin. Genet. Dev. 2*, 205−210.
7. Ellenberger, T. (1994) *Curr. Opin. Struct. Biol. 4*, 12−21.
8. Lumb, K. J., and Kim, P. S. (1995) *Science 268*, 436−439.
9. Yu, Y. H., Monera, O. D., Hodges, R. S., and Privalov, P. L. (1996) *Biophys. Chem. 59*, 299−314.
10. Lumb, K. J., and Kim, P. S. (1996) *Science 271*, 1137−1138.
11. Lavigne, P., Sonnichsen, F. D., Kay, C. M., and Hodges, R. S. (1996) *Science 271*, 1136−1137.
12. O'Shea, E. K., Lumb, K. J., and Kim, P. S. (1993) *Curr. Biol. 3*, 658−667.
13. Zhou, N. E., Kay, C. M., and Hodges, R. S. (1994) *J. Mol. Biol. 237*, 500−512.
14. Kohn, W. D., Monera, O. D., Kay, C. M., and Hodges, R. S. (1995) *J. Biol. Chem. 270*, 25495−25506.
15. Jelesarov, I., and Bosshard, H. R. (1996) *J. Mol. Biol. 263*, 344−358.
16. Wendt, H., Leder, L., Harma, H., Jelesarov, I., Baici, A., and Bosshard, H. R. (1997) *Biochemistry 36*, 204−213.
17. Lamb, P., and McKnight, S. L. (1991) *Trends Biochem. Sci. 16*, 417−422.
18. Baxevanis, A. D., and Vinson, C. R. (1993) *Curr. Opin. Genet. Dev. 3*, 278−285.
19. Zeng, X., Herndon, A. M., and Hu, J. C. (1997) *Proc. Natl. Acad. Sci. U.S.A.* 94, 3673−3678.
20. Wendt, H., Berger, C., Baici, A., Thomas, R. M., and Bosshard, H. R. (1995) *Biochemistry 34*, 4097−4107.
21. Brandts, J. F., and Kaplan, L. J. (1973) *Biochemistry 12*, 2011−2024.
22. Laue, T. M., Shah, B., Ridgeway, T. M., and Pelletier, S. L. (1992) in *Analytical ultracentrifugation in biochemistry and polymer science* (Harding, S. E., Rowe, A. J. and Horton, J. C., Eds.) pp 90−125, The Royal Society of Chemistry, Cambridge, U.K.
23. Johnson, J. S., Kraus, K. A., and Scatchard, G. (1954) *J. Phys. Chem. 58*, 1034−1039.
24. Tanford, C. (1961) *The physical chemistry of macromolecules*, Wiley, New York.
25. Durchschlag, H. (1986) in *Thermodynamic data for biochemistry and biotechnology* (Hinz, H. J., ed.), Springer-Verlag, Berlin, Germany.
26. Ellenberger, T. E., Brandl, C. J., Struhl, K., and Harrison, S. C. (1992) *Cell 71*, 1223−1237.
27. Lumb, K. J., and Kim, P. S. (1995) *Biochemistry 34*, 8642−8648.
28. Junius, F. K., Mackay, J. P., Bubb, W. A., Jensen, S. A., Weiss, A. S., and King, G. F. (1995) *Biochemistry 34*, 6164−6174.
29. Collins, K. D. (1997) *Biophys. J. 72*, 65−76.
30. Scholtz, J. M., York, E. J., Stewart, J. M., and Baldwin, R. L. (1991) *J. Am. Chem. Soc. 113*, 5102−5104.
31. Wendt, H., Baici, A., and Bosshard, H. R. (1994) *J. Am. Chem. Soc. 116*, 6973−6974.
32. Casassa, E. F., and Eisenberg, H. (1964) *Adv. Protein Chem. 19*, 287−395.
33. Arakawa, T., and Timasheff, S. N. (1985) *Methods Enzymol. 117*, 61−65.
34. Lee, J. C., Gekko, K., and Timasheff, S. N. (1979) *Methods Enzymol. 61*, 26−49.
35. Durchschlag, H., and Jaenicke, R. (1982) *Biochem. Biophys. Res. Commun. 108*, 1074−1079.

36. Pundak, S., and Eisenberg, H. (1981) *Eur. J. Biochem. 118*, 463−470.
37. Kharakoz, D. P. (1989) *Biophys. Chem. 34*, 115−125.
38. Pace, C. N. (1986) *Methods Enzymol. 131*, 266−280.
39. Marky, L. A., and Breslauer, K. J. (1987) *Biopolymers 26*, 1601−1620.
40. O'Shea, E. K., Rutkowski, R., and Kim, P. S. (1992) *Cell 68*, 699−708.
41. Hu, J. C., Newell, N. E., Tidor, B., and Sauer, R. T. (1993) *Protein Sci. 2*, 1072−1084.
42. Kohn, W. D., Kay, C. M., and Hodges, R. S. (1995) *Protein Sci. 4*, 237−250.
43. Monera, O. D., Kay, C. M., and Hodges, R. S. (1994) *Biochemistry 33*, 3862−3871.
44. Kella, N. K. D., and Kinsella, J. E. (1988) *Biochem. J. 255*, 113−118.
45. Eisenberg, H., Mevarech, M., and Zaccai, G. (1992) *Annu. Rev. Biophys. Biomol. Struct. 22*, 67−97.
46. Timasheff, S. N. (1993) *Annu. Rev. Biophys. Biomol. Struct. 22*, 67−97.
47. Von Hippel, P. H., and Wong, K. Y. (1965) *J. Biol. Chem. 240*, 3909−3923.
48. Kauzmann, W. (1959) *Adv. Protein Chem. 14*, 1−63.
49. Nemethy, G., and Scheraga, H. A. (1962) *J. Phys. Chem. 66*, 1773−1789.
50. Tanford, C. (1962) *J. Am. Chem. Soc. 84*, 4240−4247.
51. Sinanoglu, O., and Abdulnur, S. (1964) *Fed. Proc. 24 (Suppl. 15, Part 2)*, 12−23.
52. Sinanoglu, O., and Abdulnur, R. (1965) *Photochem. Photobiol. 3*, 333−342.
53. Murphy, K. P., and Freire, E. (1992) *Adv. Protein Chem. 43*, 313−361.
54. Makhatadze, G. I., and Privalov, P. L. (1995) *Adv. Protein Chem. 47*, 307−425.
55. Robinson, C. R., and Sauer, R. T. (1996) *Biochemistry 35*, 13878−13884.
56. Hoshino, M., Noboru, Y., Susumu, Y., and Goto, Y. (1997) *Protein Sci. 6*, 1396−1404.
57. Kenar, K. T., Garcia-Moreno, B., and Freire, E. (1995) *Protein Sci. 4*, 1934−1938.
58. Sturtevant, J. M. (1977) *Proc. Natl. Acad. Sci. U.S.A. 74*, 2236−2240.
59. Becktel, W. J., and Schellman, J. A. (1987) *Biopolymers 26*, 1859−1877.
60. Privalov, P. L., and Gill, S. J. (1988) *Adv. Protein Chem. 39*, 191−234.
61. Zitzewitz, J. A., Bilsel, O., Luo, J. B., Jones, B. E., and Matthews, C. R. (1995) *Biochemistry 34*, 12812−12819.
62. Munson, M., Anderson, K. S., and Regan, L. (1997) *Folding Des. 2*, 77−87.
63. Ballew, R. M., Sabelko, J., and Gruebele, M. (1996) *Proc. Natl. Acad. Sci. U.S.A. 93*, 5759−5764.
64. Ozeki, S., Kato, T., Holtzer, M. E., and Holtzer, A. (1991) *Biopolymers 31*, 957−966.
65. Wolff, J., Sackett, D. L., and Knipling, L. (1996) *Protein Sci. 5*, 2020−2028.
66. Collins, K. D., and Washabaugh, M. W. (1985) *Q. Rev. Biophys. 18*, 323−422.
67. Lee, J. D. (1990) *Concise inorganic chemistry*, Chapman and Hall, New York.

BI972977V